

## Regulation of reticular adhesions by KANK2 and talin2 in two melanoma cell lines

Anja Rac<sup>1,\*</sup> ORCID:0000-0001-8821-3059, Marija Lončarić<sup>1,\*</sup> ORCID:0000-0002-5343-0368, Nikolina Stojanović<sup>1,\*,#</sup> ORCID:0000-0002-7763-4154, Mahak Fatima<sup>2</sup> ORCID: 0000-0003-2780-0844, Mirna Rešetar<sup>1</sup>, Dalibor Hršak<sup>3</sup> ORCID: 0000-0002-1462-7424, Jonathan D. Humphries<sup>4</sup> ORCID:0000-0002-8953-7079, Martin J. Humphries<sup>2</sup> ORCID:0000-0002-4331-6967, Andreja Ambriović-Ristov<sup>1,#</sup> ORCID:0000-0001-7784-2466

<sup>1</sup>Laboratory for Cell Biology and Signalling, Division of Molecular Biology, Ruđer Bošković Institute, Zagreb, Croatia; <sup>2</sup>Manchester Cell-Matrix Centre, Faculty of Biology, Medicine & Health, University of Manchester, Manchester, United Kingdom; <sup>3</sup>Laboratory for Computational Biology and Translational Medicine, Division of Electronics, Ruđer Bošković Institute, Zagreb, Croatia; <sup>4</sup>Department of Life Science, Manchester Metropolitan University, Manchester, United Kingdom

\*equal contribution

#corresponding authors: [Nikolina.Stojanovic@irb.hr](mailto:Nikolina.Stojanovic@irb.hr), [Andreja.Ambriovic.Ristov@irb.hr](mailto:Andreja.Ambriovic.Ristov@irb.hr)

### ABSTRACT

#### ***Background***

Integrins bind extracellular matrix proteins and, upon clustering, form multimolecular integrin adhesion complexes (IACs) that connect to and regulate the cell cytoskeleton, influencing various aspects of cell behaviour. Alongside well-characterized focal adhesions (FAs) and fibrillar adhesions (FBs), a new class of IACs, reticular adhesions (RAs), have been identified. RAs, formed by integrin  $\alpha V\beta 5$ , lack actin association and classical FAs markers and their physiological role in cells remains poorly understood. Previously, we showed that two melanoma cell lines, MDA-MB-435S and RPMI-7951, preferentially use integrin  $\alpha V\beta 5$  (which can form FAs or RAs) for adhesion under long-

term culture conditions. Here we investigate the composition of RAs in these two melanoma cell lines.

### ***Methods***

Cells were treated with the actin polymerisation inhibitor cytochalasin D to disrupt FAs and enable isolation and mass spectrometry-based analysis of RAs components. Western blotting, immunofluorescence microscopy and proximity ligation assays (PLA) were performed to assess protein expression and localization within RAs. The effects of talin2 and KN motif and ankyrin repeat domains protein 2 (KANK2) knockdown on RA composition were examined in both melanoma cell lines.

### ***Results***

Known RA-associated proteins, including the Adaptor protein 2 (AP2) complex, disabled homolog 2 (DAB2), Numb and talin2 were identified in both lines, along with a new protein, KANK2. PLA following actin disruption confirmed the proximity of KANK2 and talin2 in RAs. Knockdown experiments demonstrated that although both talin2 and KANK2 are located in RAs, neither is essential for RA formation. Talin2 knockdown resulted in reduced abundance of RA components in both cell lines. In MDA-MB-435S cells, KANK2 knockdown produced a similar effect. However, in RPMI-7951 cells, KANK2 knockdown had no significant effect on RA components abundance, reflecting the differential localization and role of KANK2 in this cell line.

### ***Conclusion***

We provide a comprehensive analysis of RAs in two melanoma cell lines and identify KANK2 as a novel RA-associated protein. The differential effects of KANK2 knockdown on the abundance of RAs underscores its distinct role in  $\alpha V\beta 5$ -mediated adhesions, FAs and RAs, across the two cell lines. These findings emphasize the importance of adhesion crosstalk in regulating integrin  $\alpha V\beta 5$ -mediated cell adhesions.

### **Plain English summary**

Cells attach to their surroundings through structures called adhesions. Integrin receptor activation initiates the formation of integrin adhesion complexes at the cell membrane regulating various aspects of normal and tumour cell behaviour. In addition to well-known

adhesion types, a new kind, reticular adhesions, has recently been discovered. These adhesions are formed by the integrin  $\alpha V\beta 5$ , do not connect to the actin cytoskeleton, and differ in composition from focal adhesions. In this study, we examined reticular adhesions in two melanoma cell lines, MDA-MB-435S and RPMI-7951, which both preferentially use integrin  $\alpha V\beta 5$  for adhesion, forming focal and reticular adhesions, but differ in their ability to form fibrillar adhesions. To analyse their composition, we disrupted the actin cytoskeleton using cytochalasin D, isolated reticular adhesions and analysed them using mass spectrometry-based proteomics. Along with known reticular adhesion proteins, we identified a new protein, KN motif and ankyrin repeat domains protein KANK2, within these structures, localised in close proximity to talin2. While neither protein is essential for reticular adhesion formation, reducing talin2 levels decreased the abundance of reticular adhesion components in both cell lines. Reducing KANK2 had distinct effects: it reduced the abundance of reticular adhesions components in MDA-MB-435S cells but had little impact in RPMI-7951 cells. The differential effects of KANK2 knockdown underscores its differing roles in  $\alpha V\beta 5$ -mediated FAs across the two cell lines. These findings underscore the importance of adhesion crosstalk in regulating integrin  $\alpha V\beta 5$ -mediated cell adhesions.

## KEYWORDS

melanoma cells, reticular adhesions, talin2, KANK2, integrin  $\alpha V\beta 5$ , adhesome

## INTRODUCTION

Most cells in multicellular organisms require attachment to their surroundings through cell-cell or cell-extracellular matrix (ECM) adhesions. In cell-matrix adhesions, integrins, a family of transmembrane receptors, have long been recognized as the central scaffolds around which these complexes are built. Through binding to the ECM and clustering, integrins form multimolecular adhesion complexes [1]. The composition of integrin adhesion complexes (IACs) varies depending on the type of adhesions they form. Focal adhesions (FAs) mature from nascent adhesions and facilitate force transduction

through tight links to contractile actomyosin fibers [2, 3]. Formed by many integrin heterodimers, FAs are located primarily at the cell edge. Fibrillar adhesions (FBs), formed by integrin  $\alpha 5\beta 1$  [4], are located in the cell centre of the migrating cell [5, 6]. FBs arise through translocation of fibronectin-bound  $\alpha 5\beta 1$  integrins from the periphery to the centre [6, 7] in a tension-dependent manner and have a role in fibronectin fibrillogenesis [8, 9]. Integrins are also components of adhesion structures that lack strong actomyosin connections, are enriched in endocytic proteins [10, 11], yet still function as signalling platforms [12, 13]. These structures, formed as a result of frustrated endocytosis [14-16], and are referred to as reticular adhesions (RAs) [10], flat clathrin lattices [11, 12, 14, 17], or clathrin plaques [18-21]. RAs are mediated exclusively by integrin  $\alpha V\beta 5$  but lack most IAC components, except talin2 and tensin3 [10]. Recent studies have shown that RAs are larger than flat clathrin lattices and contain them in an interspersed manner [22]. Unlike FAs, RAs persist throughout cell division to enable effective mitosis and also transmit spatial memory from pre-mitotic to post-mitotic daughter cells [10, 23]. Since RAs form through arrested endocytosis, their core components include proteins involved in clathrin-mediated endocytosis, such as adaptor protein 2 (AP2), disabled protein 2 (Dab2), NUMB Endocytic Adaptor Protein (Numb), Epidermal Growth Factor Receptor Pathway Substrate 15 (EPS15), Epidermal Growth Factor Receptor Pathway Substrate 15 Like 1 (EPS15L1), intersectin (ITSN), and Low Density Lipoprotein Receptor Adaptor Protein 1 (LDLRAP1 or ARH) [10, 11, 14, 24]. None of these proteins are present exclusively in RAs, and therefore cannot be used as markers. Lukas et al. [25] have recently identified stonin1 as a protein exclusively present at RAs. However, they emphasized that stonin1 is not ubiquitously expressed.

Talins are key cytoplasmic mechanosensitive proteins that mediate binding of integrins to the cytoskeleton [26]. There are two different isoforms of talin: talin1 and talin2. Talin1 forms the core of FAs, increasing the affinity of integrin for ligands (integrin activation) and recruiting a range of proteins [27, 28]. Abrogation of talin1 expression leads to FA disruption, while talin2 has been shown to influence FA dynamics [29, 30]. Talin2 is mainly found at large FAs and FBs [31, 32] but also in RAs [10]. Talins directly

bind to actin and coordinate microtubule (MT) recruitment to adhesion sites via interaction with KANK proteins [26, 29, 33-35].

KANK2, a member of the KANK (kidney ankyrin repeat-containing) family proteins that bind the talin rod through a KN motif, is mainly found in mesenchymal cells [36]. Along with KANK1, KANK2 localizes to the rims of mature integrin-containing FAs and adjacent regions called cortical microtubule stabilizing complexes (CMSCs). The CMSC, recruited via KANK2-talin1 interaction [34] or talin2-KANK2 interaction [29] stabilizes MTs near mature FAs and regulates actin-microtubule crosstalk. In some cells, behind the lamella, KANK2 binding to talin promotes integrin activation, and at the same time diminishes F-actin binding to talin. Consequently, this leads to the translocation of  $\beta 1$  integrins into FBs [34]. FBs contain talin 2 [31] and KANK2 [30, 32].

RAs have been observed in various cell lines [10, 11, 25, 37]; however, information on their molecular composition has mostly come from U2OS cells [10], keratinocytes [11], and C2C12 cells [25]. Here, a comprehensive analysis of RAs in two melanoma cell lines MDA-MB-435S and RPMI-7951, which differ in their ability to form FBs in long-term culture [30], is presented. In RAs of both cell lines, previously known RA proteins, including talin2 [10], were identified, as was KANK2. Talin2 and KANK2 were not essential for RA formation in any of the analysed cell lines. Talin2 knockdown reduced the abundance of RA components in both cell lines. Surprisingly, KANK2 knockdown produced different effects on RAs depending on its preferential localization and function in the cells. In the MDA-MB-435S cell line, where KANK2 functionally interacts with talin2 in FAs [29], its knockdown produced a similar effect on RAs as talin2 knockdown. However, in RPMI-7951 cells, where KANK2 is present in FAs but also localized in FBs where it has specific function in cell migration [30], KANK2 knockdown did not affect the abundance of RA components. Our results show that talin2 and KANK2 knockdown affects RA component abundance depending on the role of these molecules within  $\alpha V\beta 5$  FAs, indicating adhesion crosstalk.

## **MATERIALS AND METHODS**

### ***Cell Cultures***

The human melanoma cell lines MDA-MB-435S and RPMI-7951 were obtained from the American Type Culture Collection (ATCC). Cells were grown on uncoated surfaces in high-glucose DMEM containing sodium bicarbonate and L-glutamine without sodium pyruvate (Sigma-Aldrich) supplemented only with 10% (v/v) FBS (Invitrogen) (DMEM-FBS) with no added antibiotics, at 37°C with 5% CO<sub>2</sub> (v/v) in a humidified atmosphere.

### ***Transient siRNA Transfection***

For transient siRNA transfection experiments, cells (MDA-MB-435S,  $4 \times 10^4$ ,  $4 \times 10^5$  or  $1.7 \times 10^6$ ; RPMI-7951,  $3.7 \times 10^4$ ,  $5 \times 10^5$  or  $1 \times 10^6$ ) were plated in 24-well, 6-well cell culture plates or 10 cm diameter Petri dishes to achieve 60–80% confluence after 24 hours. Cells were transfected 24 hours later, using Lipofectamine RNAiMax (13778150, Thermo Fisher Scientific), with 25 nM of control (Silencer™ Select Negative Control No. 1 siRNA, Ambion), ITGA5 (s7547, Ambion), ITGB5 (s7591, Ambion) or gene-specific siRNA for KANK2 (target sequence: ATGTCAACGTGCAAGATGA), TLN2 (target sequence: TTTCGTTTTTCATCTACTCCTT) [29], all purchased from Sigma. Knockdown was validated by SDS-PAGE and western blotting (WB) using specific antibodies and matched labelled secondary antibodies (See Supplementary Table S1, Supplementary Material 1).

### ***Cell treatment***

To enrich samples with RA proteins, cells were treated with different concentrations (1, 4, 7, 20 nM in DMSO) of actin polymerization inhibitor cytochalasin D (CytoD) for 2 hours at 37°C. Control cells were treated with equivalent amount of DMSO. Cells were then further processed for Mass Spectrometry (MS), WB or immunofluorescence (IF) analysis.

### ***Isolation of IACs***

IACs were isolated from cells cultivated in 10 cm diameter Petri dishes for 48 hours post-transfection for MDA-MB-435S cells or 72 hours post-transfection for RPMI-7951, with (to isolate RAs) or without CytoD treatment (to isolate all adhesions), as described previously [29, 37, 38]. Briefly, cells were washed with DMEM-HEPES and incubated with

Wang and Richard's reagent (DTBP, 6 mM, Thermo Fisher Scientific) for 10 minutes (MDA-MB-435S) or 15 minutes (RPMI-7951). DTBP is a membrane-permeable, thiol-cleavable crosslinker that covalently links proximal proteins within adhesion sites. This crosslinking step stabilizes protein-protein interactions within IACs, preserving labile or transient associations during subsequent cell lysis and wash procedures allowing efficient enrichment of IAC components while minimizing their loss or dissociation. The optimal duration of crosslinking was determined empirically based on protocol optimization by [29, 30, 37], ensuring maximal preservation of IACs without excessive crosslinking, which would introduce cytoplasmic or nuclear proteins into the samples. DTBP was quenched with 0.03M Tris-HCl (pH 8) and cells were lysed using modified RIPA buffer (50 mM Tris-HCl, pH 7.6; 150 mM NaCl; 5 mM disodium EDTA, pH 8; 1% (w/v) Triton X-100, 0.5% (w/v) SDS, 1% (w/v) sodium deoxycholate). Cell bodies were removed by high-pressure washing with tap water for 10 seconds, and remaining IACs were collected by scraping into adhesion recovery solution (125 mM Tris-HCl, pH 6.8; 1% (w/v) SDS; 150 mM dithiothreitol). Samples containing isolated IACs were acetone-precipitated and further processed for MS or WB analysis [39].

### ***Sample Preparation for MS, Data Analysis, Protein-Protein Interaction Network Analysis and Functional Enrichment Analysis***

For MS analysis, isolated IAC samples were prepared using in-gel trypsin digestion [37, 38], and analysed using a modified version of the LC-MS/MS method, as previously described [40]. Samples were analysed by LC-MS/MS using an UltiMate 3000 Rapid Separation LC (RSLC, United States) coupled to Thermo QE HF with U3000 nanoUPLC mass detector (Thermo Fisher Scientific, United States) with electrospray ionization. Peptide mixtures were eluted for 60 minutes. To identify proteins after MS analysis, data were searched against the human Swissprot and Trembl database (July 2022, July 2023) using Mascot (Matrix science, version 2.5.1). Fragment ion tolerance was set to 0.02 Da, while parent ion tolerance was 5 PPM. We set the carbamidomethylation of cysteine as a fixed modification and oxidation of methionine as a variable modification. In further analysis, we considered only peptides with ions of charge precursors 2+, 3+ and 4+.

Protein identifications were further refined using Scaffold (Proteome Software, version 5.1.0). Protein (99,9%) and peptide (90%) probabilities were assigned using the Protein Prophet algorithm [41] as incorporated by Scaffold including a minimum of four spectral counts per protein. Spectral counts were used as a measure of protein abundance. Data have been deposited in the ProteomeXchange Consortium [42] (dataset ID: PXD071922) via the PRIDE repository [43]).

Human protein-protein interactions (PPIs) were loaded from STRING database, using stringApp (confidence score cut-off = 0.40, maximum additional interactors = 0) [44] for Cytoscape software (version 3.7.1) [45]. QSpec statistical method [46] was used for MS data to measure the significance of differentially identified proteins in control cells and treated cells. For visualization of differentially expressed proteins, volcano plot (GraphPad Prism version 9.0.0 (GraphPad Software)) with the following setup was created:  $-\text{Log}(\text{FDR}) \geq 0.05$  corresponding to  $\text{FDR} \leq 0.05$ ; and fold change  $\geq 1.5$  or 2.

### ***Confocal Microscopy***

For IF analysis, cells were plated on coverslips in 24-well plates. After 48 hours, cells were fixed using ice-cold methanol for 10 minutes or 2% (v/v) paraformaldehyde for 12 minutes followed by permeabilization with 0.1% (v/v) Triton X-100 for 2 minutes, and stained with protein-specific primary antibodies for 1 hour, followed by incubation with conjugated secondary antibodies for 1 hour. The primary and secondary antibodies are listed in [Supplementary Table S1, Supplementary Material 1](#). Actin stress fibers were stained with rhodamine phalloidin (Cell Signaling Technology). Cells were mounted with DAPI Fluoromount-G (SouthernBiotech) and fluorescence and respective Interference reflection microscopy (IRM) images were acquired using an inverted confocal microscope (Leica TCS SP8 X, Leica Microsystems) with the HC PL APOCS2 63 $\times$ /1.40 oil-immersion objective, zoom set at 2 $\times$ . Images were analysed using LAS X software 3.1.1 (Leica Microsystems) and ImageJ. IRM images are included alongside each IF analysis to confirm that imaging was performed in the appropriate cellular layer containing the adhesion complexes, with the focus adjusted to the adhesion sites of cells on the upper surface of the glass coverslip.

### ***Proximity ligation assay***

Proximity ligation assay (PLA), using Duolink® PLA technology [47], was performed according to manufacturer's instructions. Briefly, cells seeded on coverslips for 48 hours were fixed, blocked and incubated with selected primary antibodies for 1 hour at 37°C in a preheated humidity chamber. Primary antibodies are listed in [Supplementary Table S1, Supplementary Material 1](#). Following washing coverslips were incubated with secondary antibodies conjugated to proprietary oligonucleotide arms (Navenibodies) for 1 hour. Incubation with specific enzymes enables the formation and amplification of a DNA circle in the spots of protein proximity. Fluorescent dots, generated by binding of fluorescently labelled probes, were visualized using an inverted confocal microscope (Leica TCS SP8 X, Leica Microsystems) with the HC PL APOCS2 63×/1.40 oil-immersion objective, zoom set at 2×. Images were analysed using LAS X software 3.1.1 (Leica Microsystems) and ImageJ.

### ***Statistical Analysis***

GraphPad Prism version 9.0.0 (GraphPad Software) was used to analyse data. Data obtained from IF or PLA assay were analysed by one-way analysis of variance (ANOVA) with Dunnett's multiple comparison, and expressed as violin or scatter plots with marked median. ns denotes not significant; \* denotes  $p < 0.05$ ; \*\* denotes  $p < 0.01$ ; \*\*\* denotes  $p < 0.001$ ; \*\*\*\* denotes  $p < 0.0001$ .

## **RESULTS**

### ***Both melanoma cell lines MDA-MB-435S and RPMI-7951 display integrin $\alpha$ V $\beta$ 5-positive, vinculin-negative structures in the cell centre***

RAs primarily require integrin  $\alpha$ V $\beta$ 5, lack association with actin, and are devoid of markers of FAs, including vinculin [10, 11]. We have previously analysed IACs of two melanoma cell lines MDA-MB-435S and RPMI-7951, grown in long-term culture, using biochemical isolation and MS-based proteomics, and demonstrated that both cell lines

preferentially use integrin  $\alpha V\beta 5$  for adhesion [30, 37]. These adhesome datasets were obtained from cells cultured for 48 hours (MDA-MB-435S) or 72 hours (RPMI-7951), on culture plates without prior ECM coating, to allow the cells to regulate their own environment by secreting ECM proteins. In these cultures, integrin  $\alpha V\beta 5$  was localized at the periphery in vinculin-positive FAs, but also in the central part of the cell in vinculin-negative structures, which were not associated with actin fibers (Fig. 1). This suggests that both melanoma cell lines, MDA-MB-435S and RPMI-7951, form RAs.

### ***Composition of IACs not associated with actin in melanoma cell lines MDA-MB-435S and RPMI-7951***

Since RAs are formed independently of the actin cytoskeleton both cell lines were exposed to CytoD, an inhibitor of actin polymerisation known to disrupt FAs, as previously described [10, 23]. To determine the optimal CytoD concentration for enriching RAs, cells were treated with increasing doses for 2 hours and IF was employed to visualize F-actin, the FA marker vinculin, the RA component Numb and the nucleus [10]. CytoD disrupted actin and FAs in a dose-dependent manner. Numb remained unaffected and progressively clustered beneath the nucleus, in a pattern characteristic of RAs. The most pronounced effect was observed at the CytoD concentration of 20  $\mu\text{M}$ , as described in [10] and was used for all subsequent experiments (See Supplementary Fig. S1, Supplementary Material 2).

Next, IACs were isolated using a previously optimized protocol [30, 37] from CytoD treated cells with enriched RAs (CytoD(+), i.e. RAs) and compared to IAC isolates from cells treated with solvent DMSO (CytoD(-), i.e. FAs and RAs). IAC isolation and LC-MS/MS analysis were performed from four biological replicates of MDA-MB-435S (See Supplementary Table S2.1., Supplementary Material 3) and RPMI-7951 (See Supplementary Table S2.2., Supplementary Material 3) cells, and spectral counts were used as a measure of protein abundance. MS analysis identified 746 proteins for MDA-MB-435S and 655 proteins for RPMI-7951 cells.

Integrin subunits that appeared in CytoD(-) samples of both cell lines were  $\alpha V$  and  $\beta 5$  (See Supplementary Table S2.1., S2.2., Supplementary Material 3), again confirming

previously published data that both cell lines preferentially use integrin  $\alpha$ V $\beta$ 5 for adhesion [29, 30, 37]. The next most abundant integrin subunit in both cell lines was  $\beta$ 1, known to pair with many different integrin  $\alpha$  subunits including  $\alpha$ V and  $\alpha$ 5 [48].

To determine the differences in IAC composition between CytoD(-) and CytoD(+) samples, in both cell lines, the method of Lock et al. [10] was employed. They defined proteins as being RA components if a greater than 2-fold increase in abundance was observed following CytoD treatment. This threshold was lowered to 1.1 since in our experiments these ratios for typical RA proteins were lower. Another reason for using a lower ratio was to enable the detection of proteins present in both FAs and RAs, such as talin2 and integrin  $\beta$ 5, and whose ratios in the MDA-MB-435S and RPMI-7951 cell lines were 1.334 and 1.225, and 1.157 and 1.272, respectively (Supplementary Table S2.3., Supplementary Material 3). This narrowed the list of candidate proteins to 225 for MDA-MB-435S cells and 430 for RPMI-7951 cells (See Supplementary Table S2.1., S2.2., Supplementary Material 3), of which 98 were shared between the cell lines (Fig. 2A, See Supplementary Table S2.3., Supplementary Material 3) and became the focus of future analysis.

A constructed Protein-Protein Interaction (PPI) network of the 98 enriched proteins (Fig. 2B; See Supplementary Table S2.1, S2.2., Supplementary Material 3) included several ECM proteins including collagen type VI alpha 3 chain (COL6A3), cysteine-rich angiogenic inducer 61 (CYR61, i.e. CCN1), thrombospondin-3 (THBS3) and Wnt family member 5A (WNT5A). Transmembrane proteins identified within the network included integrin  $\alpha$ V (ITGAV) and  $\beta$ 5 (ITGB5), apolipoprotein E (APOE), and hornerin (HRNR).

Actin and microtubule-related proteins identified within the PPI network (Fig. 2B) comprised actin-related proteins 2 and 3 (ACTR2, ACTR3), components of the Arp2/3 complex (ARPC1A, ARPC1B, ARPC2, ARPC3, ARPC4), myosin IE and myosin XVIII A (MYO1E, MYO18A), cortactin (CTTN), anillin (ANLN), talin2 (TLN2), cofilin-1 (CFL1), septin-8 (SEPTIN8) and others. It has been shown that Arp2/3-mediated actin polymerization through cortactin [49] facilitates the transition of clathrin plaques into

endocytic pits, underscoring a mechanistic role for actin in endocytosis at plaque peripheries [12].

There was also an increase in abundance of several keratins in both cell lines (Fig. 2B). Since keratins can originate from MS sample preparation contamination [50] and provide false positives, and thus far, no literature data link keratins to RAs, we did not evaluate their significance.

CytoD(+) samples in MDA-MB-435S and RPMI-7951 cells showed a higher abundance of clathrin adaptor proteins AP2A1, AP2A2, AP2B1 and AP2M1, clathrin light and heavy chains CLTA and CLTC, Numb, phosphatidylinositol-binding clathrin assembly protein (PICALM), PTB domain-containing engulfment adaptor protein 1 (GULP1), programmed cell death 6-interacting protein (PDCD6IP), SH3 domain-binding protein 4 (SH3BP4), Huntingtin-interacting protein 1 (HIP1), flotillin 1 (FLOT1), Arf-GAP domain and FG repeat-containing protein 1 (AGFG1), scaffold proteins in endocytosis intersectins 1 and 2 (ITSN1 and ITSN2), dynamin2 (DNM2) and epidermal growth factor receptor substrate 15-like 1 protein (EPS15L1) (Fig. 2B). It should be noted that, of the 98 proteins enriched upon CytoD treatment, 18 are part of the reticular adhesome determined by Lock et al. [10] (Fig. 2B (circled red); See Supplementary Table S2.4., Supplementary Material 3), and 13 of those are proteins involved in endocytosis, while the rest are actin-related. Stonin1, which has been identified as a marker for RAs [25] was identified with a low number of spectra only in MS samples of MDA-MB-435S, but not RPMI-7951 cells. This could be due to the fact that stonin1 exhibits variable expression across different human cell types [51].

MS analysis identified several ribosomal proteins (ribosomal protein large (RPL) and small (RPS)) and those related to RNA and protein synthesis such as ribosome maturation factor SBDS, RNA 2',3'-cyclic phosphate and 5'-OH ligase RTCB and proline- and glutamine-rich splicing factor SFPQ. Previous studies have described the presence of ribosomes in FAs and their transport towards adhesion sites upon binding to the ECM [52]. Ribosomal protein SA (RPSA), first identified as a laminin-binding protein, has been shown to regulate ribosome biogenesis, cytoskeletal organisation, and nuclear functions [53, 54]. It has also been implicated in cell migration [55], tumor cell blebbing and

extracellular vesicle shedding [56]. However, the role of these proteins in RA-enriched samples remains unknown.

**Supplementary Material 3 (Supplementary Tables S2.1 and S2.2)** contains quantitative MS data from four independent biological replicates per cell line, under both control and CytoD-treated conditions, along with the associated statistical evaluation. Given the quantitative nature of the MS approach, these results provide statistically significant and analytically robust evidence that constitutes the core basis of our analysis. However, to illustrate changes in protein abundance in the samples and to show the spectral count ratios used to identify proteins potentially present in RAs, **Figure 2C** displays an excerpt of number of specific spectra identified for two FA marker proteins (filamin B and talin1), two proteins found in RAs (AP2A1 and AP2A2) and integrin  $\beta 5$ , which is present in both FA and RA structures. A decrease in the abundance of filamin B and talin1 (in both cell lines) in the CytoD(+) compared to the CytoD(-) samples confirmed the loss of FAs. The sample enrichment with proteins of RAs was further demonstrated by increased ratio for AP2A1 and AP2A2 (in MDA-MB-435S), and for AP2A1 and AP2A2 and Numb (in RPMI-7951) in the CytoD(+) samples, which is in line with the literature [10, 11, 23]. Integrin  $\beta 5$  was detected in all samples (**Supplementary Tables S2.1. and S2.2., Supplementary Material 3**), consistent with its previously confirmed localization in both FAs and RAs [10, 11]. In conclusion, the results demonstrate that both MDA-MB-435S and RPMI-7951 cells form  $\alpha V\beta 5$  RAs.

Next, we isolated RAs and, following SDS-PAGE, analysed these proteins by WB on the same membrane (**Supplementary Fig. S2, S6, S7, S8, S9 Supplementary Material 2**). WB analysis also demonstrated differential protein abundance depending on whether the proteins are localized to FAs (filamin B, talin1), RAs (AP2 and Numb), both adhesion types (integrin  $\beta 5$ ), or not present/retained in IAC-enriched samples (negative control; cytosolic lactate dehydrogenase, LDH). Notably, WB robustly detected Numb, which showed enrichment following CytoD treatment in both cell lines. In RPMI-7951 cells, we additionally detected Dab2, a protein characteristic of RAs, which was not identified in the MS analysis. All antibodies used for WB demonstrated high specificity, an important point given that they were subsequently used for IF analysis.

***KANK2 is a component of RAs in MDA-MB-435S and RPMI-7951 cells***

In addition to talin2, which is known to be present in FAs and RAs [10], MS data also showed an increased abundance of KANK2 following CytoD treatment in MDA-MB-435S and RPMI-7951 cells (Fig. 3A; See Supplementary Table S2.1, S2.2., S2.3., Supplementary Material 3). KANK2 is a known interactor of talin2 [29] and these results suggest that it may represent a previously unrecognized component of RAs. WB analysis also shows KANK2 enrichment in CytoD(+) samples from both MDA-MB-435S and RPMI-7951 cells suggesting that KANK2 is present in RAs (Supplementary Fig. S2, S8, S9, Supplementary Material 2).

IF analysis demonstrated that talin2, which we recently showed to colocalize with KANK2 in both FAs and FBs [29, 30], also colocalized with KANK2 following CytoD treatment, when FAs were disrupted (Fig. 3B, D). This observation was supported by quantification showing reduced cell spreading area and the loss of FA marker vinculin in both cell lines (Fig. 3C, E). In MDA-MB-435S cells, MS analysis of four independent biological replicates yielded CytoD(+)/CytoD(-) ratios of 1.334 for talin2 and 1.262 for KANK2 (Fig. 3A), and IF analysis showed that talin2- and KANK2-positive structures persisted after CytoD treatment (Fig. 3B). Similar results were obtained in RPMI-7951 cells, with CytoD(+)/CytoD(-) ratios of 1.225 for talin2 and 1.750 for KANK2 (Fig. 3A), and persistence of talin2- and KANK2-positive structures following CytoD treatment by IF (Fig. 3D), which most likely correspond to RAs.

The main objective of our study was to demonstrate that talin2 and KANK2 localize within the same adhesion structures. To address this, we employed PLA assay, which detects proteins located within approximately 40 nm of each other. PLA analysis of talin2 and KANK2 was performed and quantified in cells before and after CytoD treatment. Appropriate PLA controls are shown in Supplementary Fig. S3, Supplementary Material 2. Following CytoD-induced actin disruption, PLA signals between talin2 and KANK2 remained detectable in RAs (Fig. 3F, G). Quantification of PLA-positive signals in both cell lines revealed that actin disruption and the concomitant loss of FAs significantly reduced,

but did not abolish, talin2-KANK2 signals (Fig. 3F, G). Overall, the persistence of talin2-KANK2 PLA signals after CytoD treatment supports their spatial association within RAs.

The adhesome of MDA-MB-435S cells contained integrin  $\beta$ 1 alongside  $\alpha$ V and  $\beta$ 5, but no spectra for integrin  $\alpha$ 5 were detected (see Supplementary Table 2.1., Supplementary Material 3), and integrin  $\alpha$ 5-positive structures characteristic of FBs were not observed (See Supplementary Fig. S4A, Supplementary Material 2). In contrast, the adhesome of RPMI-7951 cells contained  $\alpha$ V,  $\beta$ 5, and  $\beta$ 1, as well as low levels of integrin  $\alpha$ 5 (See Supplementary Table S2.2., Supplementary Material 3) and these cells formed integrin  $\alpha$ 5-positive structures characteristic of FBs (See Supplementary Fig. S4A, Supplementary Material 2). Our recent data show that RPMI-7951 cells, when cultured on uncoated surfaces, formed elongated, integrin  $\alpha$ 5-positive structures characteristic of FBs containing talin2 and KANK2 [30]. To further confirm that KANK2 and talin2 are indeed components of RAs, both cell lines were transfected with integrin subunit  $\alpha$ 5-specific siRNA, treated with CytoD (to disrupt FAs) and PLA was performed, with talin2-KANK2 PLA-positive signals subsequently quantified. The efficiency of integrin  $\alpha$ 5 knockdown in RPMI-7951 cells is shown in Supplementary Fig. S4B, Supplementary Material 2. In MDA-MB-435S cells, which do not form FBs, integrin  $\alpha$ 5 knockdown had no effect on the number of talin2-KANK2 positive signals whereas CytoD treatment caused a reduction in their number, although signals remained detectable. Similarly, in RPMI-7951 cells, integrin  $\alpha$ 5 knockdown did not significantly affect talin2-KANK2 signals, whereas CytoD treatment caused a significant reduction, although the signals remained detectable (Fig. 4A, B). Taken together, these results identify KANK2 as a previously unrecognized component of RAs.

### ***The effect of talin2 or KANK2 knockdown on RAs abundance in MDA-MB-435S and RPMI-7951 cells***

In MDA-MB-435S cells, talin2 and KANK2 within integrin  $\alpha$ V $\beta$ 5 FAs functionally interact to regulate microtubule dynamics and cell migration. More specifically, knockdown of either talin2 or KANK2 mimics the effect of integrin  $\alpha$ V or  $\beta$ 5 subunit knockdown i.e. reduces cell migration [29]. However, in RPMI-7951 cells, talin2 and

KANK2 colocalize in FAs and FBs, and their knockdown has differential effect. Talin2 knockdown mimicked the effect of  $\alpha$ V or  $\beta$ 5 integrin knockdown i.e. reduced cell migration, while KANK2 knockdown mimicked the effect of integrin  $\alpha$ 5 knockdown i.e. enhanced cell migration [30]. These findings suggest that the localization of KANK2 to FAs or FBs differentially affects cell migration [29, 30].

To investigate how talin2 or KANK2 knockdown affects their mutual localization and/or abundance in RAs, each protein was knocked down in MDA-MB-435S and RPMI-7951 cells, and cells were then exposed to CytoD. Successful knockdown was confirmed in both cell lines using three independent methods: (i) MS analysis, performed in three biological replicates for MDA-MB-435S cells and two for RPMI-7951 cells (Fig. 6; Supplementary Tables S3.1-S3.2.2, Supplementary Material 3), (ii) WB analysis of isolated IACs following talin2 or KANK2 knockdown in both cell lines (representative images of two or more WBs; Supplementary Fig. S5, S11, S12 Supplementary Material 2) and (iii) protein localization, analysed by IF and quantification of talin2 and KANK2 positive structures after talin2 or KANK2 knockdown, with the loss of vinculin signal confirming the effectiveness of the CytoD treatment (Fig. 5). After verifying the efficiency of the knockdown with these approaches, the same methods were subsequently used to assess potential changes in protein overall abundance. In MDA-MB-435S cells, talin2 knockdown was highly effective (MS, WB, IF), resulting in a slight reduction in KANK2 abundance by MS and a strong reduction in WB analysis. KANK2 knockdown was also effective (MS, WB, IF), and markedly reduced talin2 levels in MS and WB. In RPMI-7951 cells, talin2 knockdown was highly effective in MS, WB and IF, and led to decreased number of KANK2 spectra in MS (although spectral counts were low) and clearly reduced levels in WB. KANK2 knockdown in RPMI-7951 cells was successful as judged by MS, WB and IF; however, MS indicated decreased abundance, and WB analysis showed an increase in talin2 levels following KANK2 knockdown. Regarding IF quantification, which detects the number of positive structures rather than protein abundance, the results show that in MDA-MB-435S cells talin2 is reduced upon KANK2 knockdown, but not vice versa. This is in accordance to our previously published data that talin2 knockdown disrupted the link between talin2 and KANK2 in FAs but did not affect KANK2 localization [29].

Conversely, in RPMI-7951 cells knockdown of talin2 reduces KANK2 but not vice versa. This is also in accordance to our recently published data showing that KANK2 knockdown does not affect talin2 in  $\beta 5$  adhesions [30]. A major challenge in these analyses is that talin2 and KANK2 are present in all three types of adhesions, FAs, FBs, and RAs, so even a small fraction of adhesions that are not RAs (e.g., due to incomplete CytoD treatment) can affect the interpretation of data. Therefore, we conclude that knockdown of talin2 and KANK2 likely influences each other. Nevertheless, our primary goal was to assess how these knockdowns impact RA abundance, and in subsequent experiments we focused on spectral counts of proteins specifically characteristic of RAs. MS results (see Supplementary Table S3.1, S3.1.1, S3.1.2, S3.2, S3.2.1, S3.2.2., Supplementary Material 3) were processed, analysed as described above, and visualized using volcano plots. A significant change in the abundance of characteristic RA proteins was observed following talin2 knockdown in both cell lines, and after KANK2 knockdown in MDA-MB-435S, but not in the RPMI-7951 cell line (Fig. 6). In MDA-MB-435S cells, there was a significant reduction in the amount of several RA components such as AP2A1, AP2A2, EPS1L15, and ITSN2. KANK2 knockdown in MDA-MB-435S cells also led to a decrease in the level of several RA components such as CTLC proteins, AP2A1, AP2B1, and ITSN2 (Fig. 6A, B). In RPMI-7951 cells, knockdown of talin2 similarly led to a decrease in the level of RA components AP2A1, AP2A2, AP2B1, CTLC, EPS1L15 and ITSN2 (Fig. 6C, D). These results are in line with observed changes in FAs of MDA-MB-435S after either talin2 or KANK2 knockdown and RPMI-7951 cells after talin2 knockdown. It is likely that FAs become less dynamic and their size increases, but not their number, indicating a possible cause for the retention of FA proteins [29, 30], which might lead to a reduction of RAs. However, whether this is indeed the underlying mechanism remains unclear, and further studies will be required to determine whether these processes are causally linked.

KANK2 knockdown did not have the same effect as talin2 knockdown in RPMI-7951 cells. The level of the RA components AP2A1, AP2A2, AP2B1, CTLC, EPS1L15 and ITSN2 did not change (Fig. 6B). This is in line to what happens with integrin  $\alpha V\beta 5$  FAs after KANK2 knockdown. Namely, KANK2 knockdown in RPMI-7951 did not affect integrin  $\beta 5$ -positive adhesions at all [30].

## DISCUSSION

Here, we report the composition of RAs in two melanoma cell lines, MDA-MB-435S and RPMI-7951, and compare the identified components with previously published data. The findings confirm previously obtained data by Lock et al. [10] that RAs contain talin2. Additionally, KANK2 is shown to be a novel component of RAs. Given that we have extensively studied the role and localization of talin2 and KANK2 in FAs and FBs of these two cell lines [29, 30], we further analysed how the knockdown of each protein affects RAs. Our results demonstrate that talin2 and KANK2 are not essential for the formation of RAs; however, their knockdown influences RA component abundance, and primarily mirrors the roles of talin2 and KANK2 in  $\alpha$ V $\beta$ 5 FAs. This highlights the importance of adhesion crosstalk in cellular function.

The analysis of IACs in the melanoma cell lines MDA-MB-435S and RPMI-7951 demonstrated that both cell lines in long-term culture preferentially use integrin  $\alpha$ V $\beta$ 5 for adhesion, forming FAs [29, 30] and RAs (this work) that contain talin2 and KANK2. It was also found that, unlike MDA-MB-435S cells, RPMI-7951 cells form FBs that also contain talin2 and KANK2 [30]. Here RAs were analysed in both cell lines and it was demonstrated that clathrin and endocytic adaptor proteins are enriched in RA isolates as previously reported by others [10, 11, 23]. In the analysis of RA proteins, the same logic as Lock and colleagues [10] was followed; i.e. the proteins we considered to be potential RA proteins were those maintained or enriched in the sample during RA isolation. In doing so, the presence of most of the previously identified proteins was confirmed in the melanoma cells [10]. Stonin1, which has been identified as a specific adaptor for the endocytosis of NG2 and as an important factor for FA dynamics and cell migration [57], and recently shown to be as a marker for RAs [25], was only detected in RA isolates of MDA-MB-435S, with a low number of spectra. In RPMI-7951 RA isolates, stonin1 was not detected, nor was it detected in RPMI-7951 IAC isolates [30]. This could be a consequence of the protein not being expressed in abundance in the melanoma cells. Therefore, in subsequent analyses of RA levels, endocytic adaptors such as AP2 were used as markers of RAs.

Previous research identified integrin  $\alpha V\beta 5$  as the main receptor in RAs; however, it is still not clear whether  $\beta 3$  and  $\beta 1$  can also contribute to their formation [10, 11]. MS analysis of isolated IACs after disruption of actin cytoskeleton using CytoD confirmed that  $\alpha V\beta 5$  integrin preferentially forms RAs in the two melanoma cell lines. Although a small number of spectra were found for several other integrin subunits, primarily  $\beta 1$ , the  $\alpha$  subunits did not overlap between the two cell lines. In RPMI-7951 cells, but not in MDA-MB-435S cells, MS analysis identified integrin  $\alpha 5$ , which is in line with our own results that these cells form FBs [30] and can be found in RAs isolates because FBs are less dependent on actin cytoskeleton.

Talin2 was found to be unnecessary for RA maintenance, which indicates that talin2 is not an activator of integrins in RA. Potential activators of integrin  $\beta 5$  in RA include the proteins Dab2, Numb, and ARH, which have been shown to interact directly with integrin  $\beta 5$  [58], and whose binding affinity for integrin  $\beta 5$  is several times higher than that of talin1 [23].

The key finding here is that KANK2 is a component of RAs in both melanoma cell lines. Not only was KANK2 enriched in samples of isolated RAs from both cell lines, those that form FBs and those that do not, but PLA analysis after integrin  $\alpha 5$  knockdown (to deplete FBs) and CytoD treatment (to deplete FAs) also revealed close proximity between talin2 and KANK2. Therefore, given that talin2 and KANK2 were found in three different types of adhesions, this suggests that they may play a role in the interconversion. The fate of FAs and RAs has been suggested to be mainly connected via their shared use of  $\alpha V\beta 5$  integrins. Manipulations that inhibited one of these structures appeared to favour the other [10, 25] presumably by enlarging the available  $\alpha V\beta 5$  integrin pool [25]. Our results support these data. Namely, in MDA-MB-435S cell line talin2 from integrin  $\alpha V\beta 5$  FAs and KANK2 from CMSC have been implicated in maintaining actin-MT crosstalk. Therefore, knockdown of either of these proteins alters integrin  $\alpha V\beta 5$  FAs dynamics, resulting in enlarged  $\alpha V\beta 5$  FAs along with reduced cell migration [29]. The enlarged  $\alpha V\beta 5$  FAs suggest increased levels of FA proteins. Therefore, it was not surprising that knockdown of either talin2 or KANK2 led to reduced abundance of RA components. In RPMI-7951 cells, which form three talin2 and KANK2 positive adhesions (FAs, FBs and RAs), talin2 knockdown

also increased FA size (suggesting increased levels of FA proteins) and reduced cell migration [30], and again a reduction in RAs levels was observed. However, in the RPMI-7951 cell line, KANK2 knockdown did not affect integrin  $\alpha$ V $\beta$ 5 FAs. Therefore, the unaltered  $\alpha$ V $\beta$ 5 FAs likely explains why the abundance of RA components remains unchanged after KANK2 knockdown.

The MS-data analysis showed that in MDA-MB-435S cells (which lack FBs), talin2 knockdown did not affect KANK2 levels, although the characteristic RA proteins were reduced. In RPMI-7951 cells, the very low number of KANK2-specific spectra made it impossible to determine whether KANK2 levels change; however, a clear decrease in specific RA proteins was observed. However, we believe that these data do not imply that KANK2 is not a part of RAs. Still, it remains unclear whether talin2 and KANK2 directly interact within RAs and what functional role they might play. Conversely, in both melanoma cell lines, KANK2 knockdown reduced talin2 levels, regardless of the overall effect on RA-specific proteins. This finding suggests the talin2 dependence of KANK2 levels. Moreover, it is in line with the previously mentioned observation that RA formation is independent of both talin2, already observed by [10], and apparently, KANK2 (our own data).

Until recently, it was not clear how  $\alpha$ V $\beta$ 5 integrin physically transfers between FAs and RAs. It has been shown that RAs arise more frequently at sites where the FA marker paxillin was progressively replaced by stonin1. In addition, the conversions in the opposite direction also occur by the recruitment of paxillin onto pre-existing  $\beta$ 5 integrin scaffolds. These data indicate that two integrin  $\alpha$ V $\beta$ 5-based adhesions, having distinct molecular compositions, are intimately linked and dynamically interconvertible [25]. FAs and RAs are inversely regulated complexes and the balance between these types of adhesions is influenced by phosphatidylinositols [10]. High levels of activated myosin light chain (p-MLC) also correlated with integrin  $\alpha$ V $\beta$ 5 localizing to FAs over RAs [23]. Decreased membrane tension together with formation of contractile stress fibers, promotes the assembly of FAs, reduces RAs, and decreases cancer cell migration [59]. In MDA-MB-435S cells talin2 knockdown enhanced stress fiber formation and reduced cell migration. In addition, talin2 knockdown increased the size of FAs indicating preference of  $\alpha$ V $\beta$ 5 for

FAs over RAs [29]. Therefore, our results are consistent with this mechanism of inverse regulation of FA and RA. These conclusions are further supported by results in the RPMI-7951 cell line, in which only talin2 alters FAs and consequently alters RAs.

This comprehensive analysis of RAs in two melanoma cell lines expands on previous findings and highlights novel molecular components. The presence of talin2 in RAs is confirmed and KANK2 is identified as a novel RA-associated protein in both cell lines. While neither protein is essential for RA formation, their knockdown significantly alters RA abundance and composition, reflecting their broader roles in other adhesion types such as FAs and FBs. These findings emphasize the importance of adhesion crosstalk and the dynamic balance between different adhesion structures, which is influenced by integrin composition, cytoskeletal integrity, and membrane tension.

#### **List of abbreviations**

IAC Integrin adhesion complex

FA Focal adhesion

FB Fibrillar adhesion

RA Reticular adhesion

CytoD Cytochalasin D

PLA Proximity ligation assay

KANK KN motif and ankyrin repeat domain containing protein

ECM Extracellular matrix

AP2 Adaptor protein 2

DAB2 Disabled homolog 2

NUMB Endocytic Adaptor Protein Numb

EPS15 Epidermal Growth Factor Receptor Pathway Substrate

ITSN Intersectin (ITSN)

LDLRAP1 Low Density Lipoprotein Receptor Adaptor Protein 1

MT Microtubule

CMSC Cortical microtubule stabilizing complex

ATCC American Type Culture Collection

DMEM Dulbecco's Modified Eagle Medium

FBS Fetal Bovine Serum

ITGA5 Integrin Subunit  $\alpha$ 5

ITGB5 Integrin Subunit  $\beta$ 5

TLN2 Talin2

WB Western blotting

MS Mass spectrometry

IF Immunofluorescence analysis

HEPES Hydroxyethylpiperazine ethanesulfonic acid

DTBP Dimethyl 3,3'-dithiobispropionimidate, Wang and Richard's reagent

LC-MS Liquid Chromatography-Mass Spectrometry

PRIDE PRoteomics IDentifications Database

PPI network Protein-Protein Interaction Network

STRING Search Tool for the Retrieval of Interacting Genes/Proteins

SDS-PAGE sodium dodecyl sulfate-polyacrylamide gel electrophoresis

IRM Interference reflection microscopy

SD Standard Deviation

COL6A3 Collagen type VI alpha 3 chain

CCN1 Cysteine-rich angiogenic inducer 61 CYR61

THBS3 Thrombospondin-3

WNT5A Wnt family member 5A

APOE Apolipoprotein E

HRNR Hornerin

ITGAV Integrin  $\alpha$ V

ACTR2 Actin-related protein 2

ACTR3 Actin-related protein3

ARPC1A Actin Related Protein 2/3 Complex Subunit 1A

ARPC1B Actin Related Protein 2/3 Complex Subunit 1B

ARPC2 Actin Related Protein 2/3 Complex Subunit 2

ARPC3 Actin Related Protein 2/3 Complex Subunit 3  
ARPC4 Actin Related Protein 2/3 Complex Subunit 4  
MYO1E Myosin IE  
MYO18A Myosin XVIIIIA  
CTTN Cortactin  
ANLN Anillin  
CFL1 Cofilin-1  
SEPTIN8 Septin-8  
AP2A1 Adaptor Related Protein Complex 2 Subunit Alpha 1  
AP2A2 Adaptor Related Protein Complex 2 Subunit Alpha 1  
AP2B1 Adaptor Related Protein Complex 2 Subunit Beta 1  
AP2M1 Adaptor Related Protein Complex 2 Subunit Mu 1  
CLTA Clathrin light chain  
CLTC Clathrin heavy chain  
PICALM Phosphatidylinositol-binding clathrin assembly protein  
GULP1 PTB domain-containing engulfment adaptor protein 1  
PDCD6IP Programmed cell death 6-interacting protein  
SH3BP4 SH3 domain-binding protein 4  
HIP1 Huntingtin-interacting protein 1  
FLOT1 Flotillin 1  
AGFG1 Arf-GAP domain and FG repeat-containing protein 1  
ITSN1 Intersectin 1  
ITSN2 Intersectin 2  
DNM2 Dynamin2  
EPS15L1 Epidermal growth factor receptor substrate 15-like 1 protein  
RPL Ribosomal protein large  
RPS Ribosomal protein small  
SBDS Ribosome maturation factor  
RTCB RNA 2',3'-cyclic phosphate and 5'-OH ligase  
SFPQ Proline- and glutamine-rich splicing factor

RPSA Ribosomal protein SA

## **Declarations**

### **Ethics approval and consent to participate**

Not applicable

### **Consent for publication**

Not applicable

### **Availability of data and materials**

The datasets supporting the conclusions of this article are available in the ProteomeXchange Consortium via the PRIDE partner repository, dataset identifier PXD071922, <https://www.ebi.ac.uk/pride/archive/>. Other raw data supporting the conclusions of this article will be made available by the authors, without undue reservation, to any qualified researcher.

### **Competing interests**

The authors have no competing interests to disclose.

### **Funding**

This work was supported by the Croatian Science Foundation Project (Grant No IP-2019-04-1577 to AA-R), a Cancer Research UK Programme Grant to MJH (DRCRPG-100002) and an Academy of Medical Science Springboard award to JDH (SBF008\1094).

### **Author contributions**

[AR], [ML] and [NS] contributed equally to the experimental work and share first authorship. Material preparation, data collection and analysis were performed by [AR], [ML], [NS], [MF], [MR], [DH], and [AA-R]. The first draft of the manuscript was written by [NS] and [AA-R], corrections were made by [AR], [ML], [JDH] and [MJH]. All authors

read and approved the final manuscript. [NS] and [AA-R] equally contributed to the study conception and design.

### **Acknowledgements**

We thank Marina Šutalo of the Laboratory for Cell Biology and Signalling for technical assistance.

### **Authors' information (optional)**

Not applicable

### **REFERENCES**

1. Chastney MR, Conway JRW, Ivaska J. Integrin adhesion complexes. *Current Biology*. 2021;31(10):R536-R42.
2. Mishra YG, Manavathi B. Focal adhesion dynamics in cellular function and disease. *Cell Signal*. 2021;85:110046.
3. Yamaguchi N, Knaut H. Focal adhesion-mediated cell anchoring and migration: from in vitro to in vivo. *Development*. 2022;149(10).
4. Conway JRW, Jacquemet G. Cell matrix adhesion in cell migration. *Essays Biochem*. 2019;63(5):535-51.
5. Katz BZ, Zamir E, Bershadsky A, Kam Z, Yamada KM, Geiger B. Physical state of the extracellular matrix regulates the structure and molecular composition of cell-matrix adhesions. *Mol Biol Cell*. 2000;11(3):1047-60.
6. Pankov R, Cukierman E, Katz BZ, Matsumoto K, Lin DC, Lin S, et al. Integrin dynamics and matrix assembly: tensin-dependent translocation of alpha(5)beta(1) integrins promotes early fibronectin fibrillogenesis. *J Cell Biol*. 2000;148(5):1075-90.
7. Clark K, Pankov R, Travis MA, Askari JA, Mould AP, Craig SE, et al. A specific alpha5beta1-integrin conformation promotes directional integrin translocation and fibronectin matrix formation. *J Cell Sci*. 2005;118(Pt 2):291-300.

8. Zamir E, Katz M, Posen Y, Erez N, Yamada KM, Katz BZ, et al. Dynamics and segregation of cell-matrix adhesions in cultured fibroblasts. *Nat Cell Biol.* 2000;2(4):191-6.
9. Lu J, Doyle AD, Shinsato Y, Wang S, Bodendorfer MA, Zheng M, et al. Basement Membrane Regulates Fibronectin Organization Using Sliding Focal Adhesions Driven by a Contractile Winch. *Dev Cell.* 2020;52(5):631-46 e4.
10. Lock JG, Jones MC, Askari JA, Gong X, Oddone A, Olofsson H, et al. Reticular adhesions are a distinct class of cell-matrix adhesions that mediate attachment during mitosis. *Nat Cell Biol.* 2018;20(11):1290-302.
11. Zuidema A, Wang W, Kreft M, Te Molder L, Hoekman L, Bleijerveld OB, et al. Mechanisms of integrin  $\alpha$ V $\beta$ 5 clustering in flat clathrin lattices. *J Cell Sci.* 2018;131(21).
12. Leyton-Puig D, Isogai T, Argenzio E, van den Broek B, Klarenbeek J, Janssen H, et al. Flat clathrin lattices are dynamic actin-controlled hubs for clathrin-mediated endocytosis and signalling of specific receptors. *Nat Commun.* 2017;8:16068.
13. Alfonzo-Mendez MA, Sochacki KA, Strub MP, Taraska JW. Dual clathrin and integrin signaling systems regulate growth factor receptor activation. *Nat Commun.* 2022;13(1):905.
14. Baschieri F, Dayot S, Elkhatib N, Ly N, Capmany A, Schauer K, et al. Frustrated endocytosis controls contractility-independent mechanotransduction at clathrin-coated structures. *Nat Commun.* 2018;9(1):3825.
15. Baschieri F, Porshneva K, Montagnac G. Frustrated clathrin-mediated endocytosis - causes and possible functions. *J Cell Sci.* 2020;133(11).
16. Bruna-Gauchoux J, Montagnac G. Constraints and frustration in the clathrin-dependent endocytosis pathway. *C R Biol.* 2022;345(2):43-56.
17. De Deyne PG, O'Neill A, Resneck WG, Dmytrenko GM, Pumplin DW, Bloch RJ. The vitronectin receptor associates with clathrin-coated membrane domains via the cytoplasmic domain of its  $\beta$ 5 subunit. *J Cell Sci.* 1998;111 ( Pt 18):2729-40.
18. Saffarian S, Cocucci E, Kirchhausen T. Distinct dynamics of endocytic clathrin-coated pits and coated plaques. *PLoS Biol.* 2009;7(9):e1000191.

19. Lampe M, Vassilopoulos S, Merrifield C. Clathrin coated pits, plaques and adhesion. *J Struct Biol.* 2016;196(1):48-56.
20. Bucher D, Mukenhirn M, Sochacki KA, Saharuka V, Huck C, Zambarda C, et al. Focal adhesion-generated cues in extracellular matrix regulate cell migration by local induction of clathrin-coated plaques. *bioRxiv.* 2018:493114.
21. Moulay G, Laine J, Lemaitre M, Nakamori M, Nishino I, Caillol G, et al. Alternative splicing of clathrin heavy chain contributes to the switch from coated pits to plaques. *J Cell Biol.* 2020;219(9).
22. Hakanpaa L, Abouelezz A, Lenaerts AS, Culfa S, Algie M, Barlund J, et al. Reticular adhesions are assembled at flat clathrin lattices and opposed by active integrin alpha5beta1. *J Cell Biol.* 2023;222(8).
23. Zuidema A, Wang W, Kreft M, Bleijerveld OB, Hoekman L, Aretz J, et al. Molecular determinants of alphaVbeta5 localization in flat clathrin lattices - role of alphaVbeta5 in cell adhesion and proliferation. *J Cell Sci.* 2022;135(11).
24. Lock JG, Baschieri F, Jones MC, Humphries JD, Montagnac G, Stromblad S, et al. Clathrin-containing adhesion complexes. *J Cell Biol.* 2019;218(7):2086-95.
25. Lukas F, Matthaeus C, Lopez-Hernandez T, Lahmann I, Schultz N, Lehmann M, et al. Canonical and non-canonical integrin-based adhesions dynamically interconvert. *Nat Commun.* 2024;15(1):2093.
26. Klapholz B, Brown NH. Talin - the master of integrin adhesions. *J Cell Sci.* 2017;130(15):2435-46.
27. del Rio A, Perez-Jimenez R, Liu R, Roca-Cusachs P, Fernandez JM, Sheetz MP. Stretching single talin rod molecules activates vinculin binding. *Science.* 2009;323(5914):638-41.
28. Goult BT, Brown NH, Schwartz MA. Talin in mechanotransduction and mechanomemory at a glance. *J Cell Sci.* 2021;134(20).
29. Loncaric M, Stojanovic N, Rac-Justament A, Coopmans K, Majhen D, Humphries JD, et al. Talin2 and KANK2 functionally interact to regulate microtubule dynamics, paclitaxel sensitivity and cell migration in the MDA-MB-435S melanoma cell line. *Cell Mol Biol Lett.* 2023;28(1):56.

30. Stojanović N, Rac A, Lončarić M, Tadijan A, Paradžik M, Acman M, et al. KANK2 at focal adhesion regulates their maintenance and dynamics, while at fibrillar adhesions it influences cell migration via microtubule-dependent mechanism. *bioRxiv*. 2025:2025.02.24.639831.
31. Praekelt U, Kopp PM, Rehm K, Linder S, Bate N, Patel B, et al. New isoform-specific monoclonal antibodies reveal different sub-cellular localisations for talin1 and talin2. *Eur J Cell Biol*. 2012;91(3):180-91.
32. Atherton P, Konstantinou R, Neo SP, Wang E, Balloi E, Ptushkina M, et al. Tensin3 interaction with talin drives the formation of fibronectin-associated fibrillar adhesions. *J Cell Biol*. 2022;221(10).
33. Bouchet BP, Gough RE, Ammon YC, van de Willige D, Post H, Jacquemet G, et al. Talin-KANK1 interaction controls the recruitment of cortical microtubule stabilizing complexes to focal adhesions. *Elife*. 2016;5.
34. Sun Z, Tseng HY, Tan S, Senger F, Kurzawa L, Dedden D, et al. Kank2 activates talin, reduces force transduction across integrins and induces central adhesion formation. *Nat Cell Biol*. 2016;18(9):941-53.
35. Goult BT, Yan J, Schwartz MA. Talin as a mechanosensitive signaling hub. *J Cell Biol*. 2018;217(11):3776-84.
36. Chen NP, Sun Z, Fassler R. The Kank family proteins in adhesion dynamics. *Curr Opin Cell Biol*. 2018;54:130-6.
37. Paradzik M, Humphries JD, Stojanovic N, Nestic D, Majhen D, Dekanic A, et al. KANK2 Links alphaVbeta5 Focal Adhesions to Microtubules and Regulates Sensitivity to Microtubule Poisons and Cell Migration. *Front Cell Dev Biol*. 2020;8:125.
38. Jones MC, Humphries JD, Byron A, Millon-Fremillon A, Robertson J, Paul NR, et al. Isolation of integrin-based adhesion complexes. *Curr Protoc Cell Biol*. 2015;66:9 8 1-9 8 15.
39. Robertson J, Jacquemet G, Byron A, Jones MC, Warwood S, Selley JN, et al. Defining the phospho-adhesome through the phosphoproteomic analysis of integrin signalling. *Nat Commun*. 2015;6:6265.

40. Horton ER, Byron A, Askari JA, Ng DHJ, Millon-Fremillon A, Robertson J, et al. Definition of a consensus integrin adhesome and its dynamics during adhesion complex assembly and disassembly. *Nat Cell Biol.* 2015;17(12):1577-87.
41. Nesvizhskii AI, Keller A, Kolker E, Aebersold R. A statistical model for identifying proteins by tandem mass spectrometry. *Anal Chem.* 2003;75(17):4646-58.
42. Deutsch EW, Bandeira N, Perez-Riverol Y, Sharma V, Carver JJ, Mendoza L, et al. The ProteomeXchange consortium at 10 years: 2023 update. *Nucleic Acids Res.* 2023;51(D1):D1539-D48.
43. Perez-Riverol Y, Bandla C, Kundu DJ, Kamatchinathan S, Bai J, Hewapathirana S, et al. The PRIDE database at 20 years: 2025 update. *Nucleic Acids Res.* 2025;53(D1):D543-D53.
44. Doncheva NT, Morris JH, Gorodkin J, Jensen LJ. Cytoscape StringApp: Network Analysis and Visualization of Proteomics Data. *J Proteome Res.* 2019;18(2):623-32.
45. Shannon P, Markiel A, Ozier O, Baliga NS, Wang JT, Ramage D, et al. Cytoscape: a software environment for integrated models of biomolecular interaction networks. *Genome Res.* 2003;13(11):2498-504.
46. Choi H, Fermin D, Nesvizhskii AI. Significance analysis of spectral count data in label-free shotgun proteomics. *Mol Cell Proteomics.* 2008;7(12):2373-85.
47. Alam MS. Proximity Ligation Assay (PLA). *Curr Protoc Immunol.* 2018;123(1):e58.
48. Arias-Mejias SM, Warda KY, Quattrocchi E, Alonso-Quinones H, Somnidi-Damodaran S, Meves A. The role of integrins in melanoma: a review. *Int J Dermatol.* 2020;59(5):525-34.
49. Uruno T, Liu J, Zhang P, Fan Y, Egile C, Li R, et al. Activation of Arp2/3 complex-mediated actin polymerization by cortactin. *Nat Cell Biol.* 2001;3(3):259-66.
50. Hodge K, Have ST, Hutton L, Lamond AI. Cleaning up the masses: exclusion lists to reduce contamination with HPLC-MS/MS. *J Proteomics.* 2013;88:92-103.
51. Lukas F, Duchmann M, Maritzen T. Focal adhesions, reticular adhesions, flat clathrin lattices: what divides them, what unites them? *Am J Physiol Cell Physiol.* 2025;328(1):C288-C302.

52. Simpson LJ, Reader JS, Tzima E. Mechanical Forces and Their Effect on the Ribosome and Protein Translation Machinery. *Cells*. 2020;9(3).
53. Mercurio AM. Laminin receptors: achieving specificity through cooperation. *Trends Cell Biol*. 1995;5(11):419-23.
54. DiGiacomo V, Meruelo D. Looking into laminin receptor: critical discussion regarding the non-integrin 37/67-kDa laminin receptor/RPSA protein. *Biol Rev Camb Philos Soc*. 2016;91(2):288-310.
55. Lefebvre T, Rybarczyk P, Bretaudeau C, Vanlaeys A, Cousin R, Brassart-Pasco S, et al. TRPM7/RPSA Complex Regulates Pancreatic Cancer Cell Migration. *Front Cell Dev Biol*. 2020;8:549.
56. Brassart B, Da Silva J, Donet M, Seurat E, Hague F, Terryn C, et al. Tumour cell blebbing and extracellular vesicle shedding: key role of matrikines and ribosomal protein SA. *Br J Cancer*. 2019;120(4):453-65.
57. Feutlinske F, Browarski M, Ku MC, Trnka P, Waiczies S, Niendorf T, et al. Stonin1 mediates endocytosis of the proteoglycan NG2 and regulates focal adhesion dynamics and cell motility. *Nat Commun*. 2015;6:8535.
58. Calderwood DA, Fujioka Y, de Pereda JM, Garcia-Alvarez B, Nakamoto T, Margolis B, et al. Integrin beta cytoplasmic domain interactions with phosphotyrosine-binding domains: a structural prototype for diversity in integrin signaling. *Proc Natl Acad Sci U S A*. 2003;100(5):2272-7.
59. Djakbarova U, Madraki Y, Chan ET, Wu T, Atreaga-Muniz V, Akatay AA, et al. Tension-induced adhesion mode switching: the interplay between focal adhesions and clathrin-containing adhesion complexes. *bioRxiv*. 2024:2024.02.07.579324.

## FIGURE LEGENDS

Fig. 1 Melanoma cell lines MDA-MB-435S and RPMI-7951 contain integrin  $\beta$ 5-positive, vinculin- and F-actin-negative structures in the cell centre. Forty-eight hours after seeding, cells were fixed with 4% PFA, and stained with anti-integrin  $\beta$ 5 antibody followed by Alexa-Fluor 647-conjugated antibody (magenta) and anti-vinculin Alexa-Fluor 555-conjugated primary antibody (red). F-actin staining (green) was performed and IRM images were taken. Analysis was performed using TCS SP8 Leica. Scale bar = 10  $\mu$ m.

Fig. 2 MS analysis of RAs isolated from MDA-MB-435S and RPMI-7951 melanoma cell lines. (A) Venn diagram represents the number of RA proteins enriched only in MDA-MB-435S cells (orange) and the number of RA proteins enriched only in RPMI-7951 cells (grey). Enriched RA proteins found in both cell lines are shown in the intersected white area of the diagram. (B) PPI network identified by MS in RAs isolated from both MDA-MB-435S and RPMI-7951 cells. Identified proteins are labelled with gene symbols, arranged and coloured according to their functional group as indicated. (C) Excerpt from MS data (See Supplementary Table S2.1 and S2.2., Supplementary Material 3) showing the number of protein-specific spectra for FAs proteins (red), RAs proteins (green) and integrin  $\beta$ 5 present in both FAs and RAs (black). Dataset consists of four replicas. CytoD(+)/CytoD(-) ratio shown.

Fig. 3 KANK2 colocalizes with talin2 in vinculin-negative structures in two melanoma cell lines MDA-MB-435S and RPMI-7951. (A) Excerpt from MS data (See Supplementary Table S2.1 and S2.2., Supplementary Material 3) showing the number of spectra specific for talin2 and KANK2 in MDA-MB-435S and RPMI-7951 cells. Dataset consists of four replicas. CytoD(+)/CytoD(-) ratio shown for both cell lines. (B, D) Talin2 and KANK2 are localized within RAs of both cell lines. Forty-eight hours after seeding, and 2 hours after CytoD treatment, cells were methanol fixed, stained with anti-vinculin Alexa-Fluor 555-conjugated primary antibody (red), anti-talin2 antibody followed by Alexa-Fluor IgG2b 488-conjugated antibody (green) and anti-KANK2 antibody followed by Alexa-Fluor 647-conjugated antibody (magenta). IRM images were taken. Analysis was performed using

TCS SP8 Leica. Scale bar = 10  $\mu$ m. (C, E) Quantification of data presented in (B, D) respectively. Violin plots (number of structures/cell) and scatter plots (cell spreading area) with marked median represent measurements of > 40 cells. Data were analysed by one-way ANOVA with Dunnett's multiple comparison. ns, not significant; \*  $P < 0.05$ ; \*\*  $P < 0.01$ ; \*\*\*  $P < 0.001$ ; \*\*\*\*  $P < 0.0001$ . (F, G) Talin2 and KANK2 are in close proximity in RAs of both cell lines. Forty-eight hours after seeding, and 2 hours after CytoD treatment, RPMI-7951 cells were methanol fixed, and a PLA assay with anti-talin2 and anti-KANK2 primary antibody was performed. Generated fluorescent dots were visualized and IRM images were taken. Analysis was performed using TCS SP8 Leica. Scale bar = 10  $\mu$ m. Quantification of data is presented in scatter plots with marked median (measurements of > 60 cells). Data were analysed by one-way ANOVA with Dunnett's multiple comparison. ns, not significant; \*  $P < 0.05$ ; \*\*  $P < 0.01$ ; \*\*\*  $P < 0.001$ ; \*\*\*\*  $P < 0.0001$ .

Fig. 4 KANK2 is a component of RAs in two melanoma cell lines. Talin2 and KANK2 are in close proximity in RAs of both cell lines. Forty-eight hours after transfection with either control siRNA (si(-)) or integrin  $\alpha$ 5-specific siRNA (si(ITGA5)), followed by 2 hours CytoD treatment, cells were methanol fixed, and a PLA assay with anti-talin2 and anti-KANK2 primary antibody was performed. Generated fluorescent dots were visualized and IRM images were taken. Analysis was performed using TCS SP8 Leica. Scale bar = 10  $\mu$ m. Quantification of data is presented in scatter plots with marked median (measurements of > 40 cells). Data were analysed by one-way ANOVA with Dunnett's multiple comparison. ns, not significant; \*  $P < 0.05$ ; \*\*  $P < 0.01$ ; \*\*\*  $P < 0.001$ ; \*\*\*\*  $P < 0.0001$ .

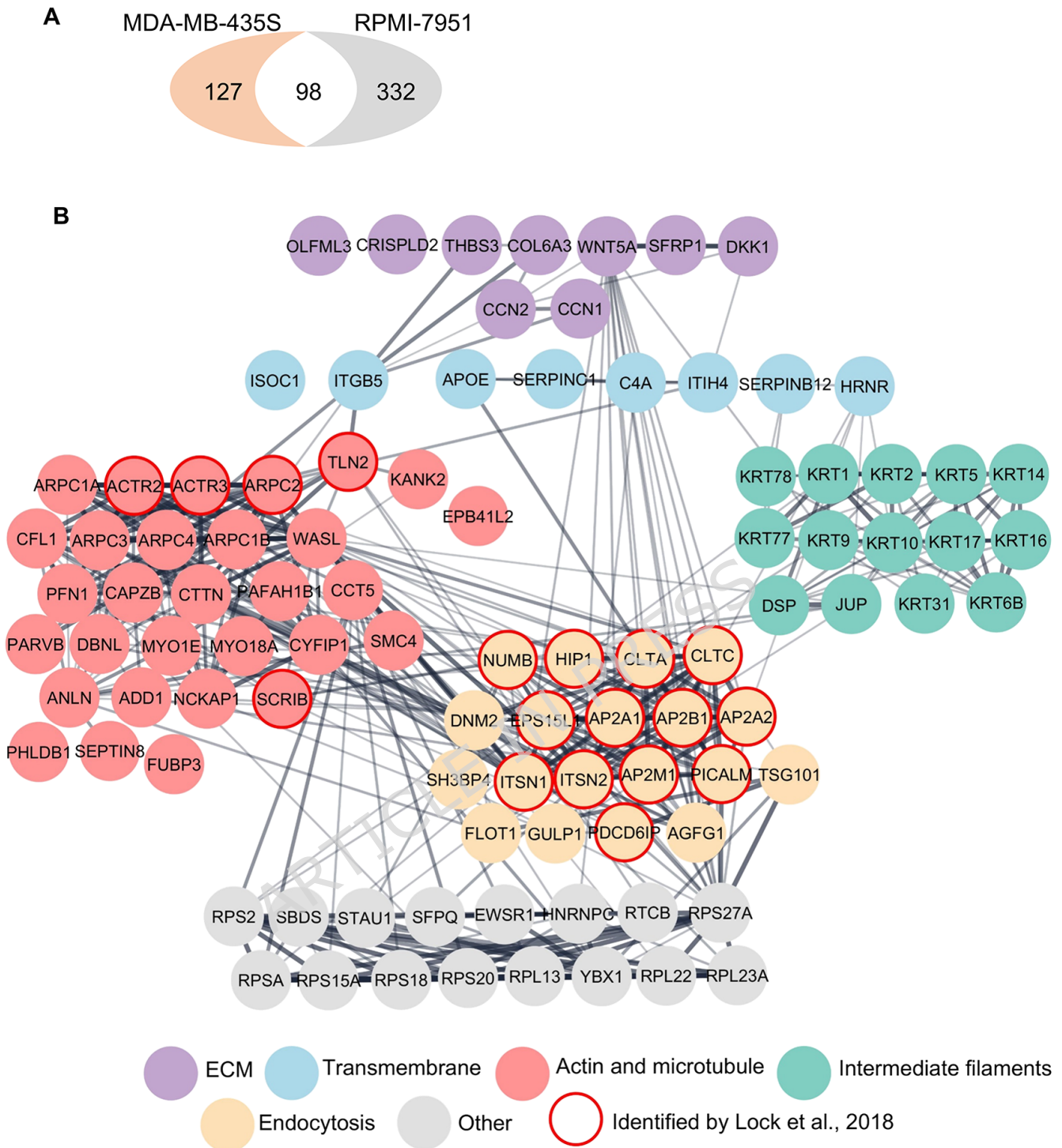
Fig. 5 Neither talin2 nor KANK2 are essential for RA maintenance. Forty-eight hours after transfection with either control siRNA (si(-)), talin2-specific (si(talin2)) or KANK2-specific (si(KANK2)) siRNA, followed by 2 hours CytoD treatment, MDA-MB-435S (A) and RPMI-7951 (C) cells were methanol fixed, and stained with anti-vinculin Alexa-Fluor 555-conjugated primary antibody (red), anti-talin2 antibody followed by Alexa-Fluor IgG2b 488-conjugated antibody (green) and anti-KANK2 antibody followed by Alexa-Fluor 647-conjugated antibody (magenta). IRM images were taken. Analysis was performed using

TCS SP8 Leica. Scale bar = 10  $\mu$ m. (B, D) Quantification of data presented in (A, C) respectively. Violin plots represent measurements of > 40 cells. Data were analysed by one-way ANOVA with Dunnett's multiple comparison. ns, not significant; \*  $P < 0.05$ ; \*\*  $P < 0.01$ ; \*\*\*  $P < 0.001$ ; \*\*\*\*  $P < 0.0001$ .

Fig. 6 Talin2 and KANK2 knockdown differentially alters RA component abundance in MDA-MB-435S versus RPMI-7951 cells. Volcano plot analysis of proteins detected in RAs isolated from (A) MDA-MB-435S and (C) RPMI-7951 cells transiently transfected with control siRNA (si(-)) versus talin2-specific siRNA (si(talin2)) or KANK2-specific siRNA (si(KANK2)). RA proteins are visualized as volcano plot after the analysis with QSpec/QProt to generate  $-\log(\text{FDR})$  and fold change values. Cut off values of  $-\log(\text{FDR}) \geq 0.05$  (red horizontal dotted line) corresponding to  $\text{FDR} \leq 0.05$ ; and fold change  $\geq 1.5$  (black vertical dotted line) or 2 (red vertical dotted line) were used. Each dot on the plot represents one protein. Proteins with significantly different abundance between RAs of si(talin2) or si(KANK2) and si(-) cells and of interest for this paper were marked with their gene name (green). Upper left quadrant - proteins detected with lower levels of spectra in si(talin2), upper right quadrant - proteins detected with higher levels of spectra in si(talin2) or si(KANK2). (B, D) Excerpt from MS data (See Supplementary Table S3.1 and S3.2., Supplementary Material 3) showing number of specific spectra for proteins presented in volcano plots (A, C) upon talin2 or KANK2 knockdown. Dataset consists of three replicas for MDA-MB-435S cells (B) and two replicas for RPMI-7951 cells (D). si(-)/si(talin2) or si(KANK2) ratio shown.



Fig. 2

**C**

PROTEIN		CytoD(-)	CytoD(+)	CytoD(+) /CytoD(-)		CytoD(-)	CytoD(+)	CytoD(+) /CytoD(-)
Filamin B	MDA-MB-435S	212/24/120/32	143/7/44/6	0.515	RPMI-7951	314/131/176/252	115/110/175/142	0.621
Talin1		218/118/160/111	165/108/167/80	0.857		219/106/131/164	192/95/147/104	0.868
AP2A1		24/9/10/2	49/15/25/3	2.044		25/12/23/25	19/30/36/27	1.318
AP2A2		13/0/0/0	34/0/16/0	3.846		15/0/10/12	22/13/34/16	2.297
Integrin $\beta$ 5		64/73/52/40	64/77/79/45	1.157		43/8/15/37	27/15/43/46	1.272
Numb		0/0/0/0	4/0/0/0	NA*		3/1/1/0	5/3/5/0	2.600

Fig. 3

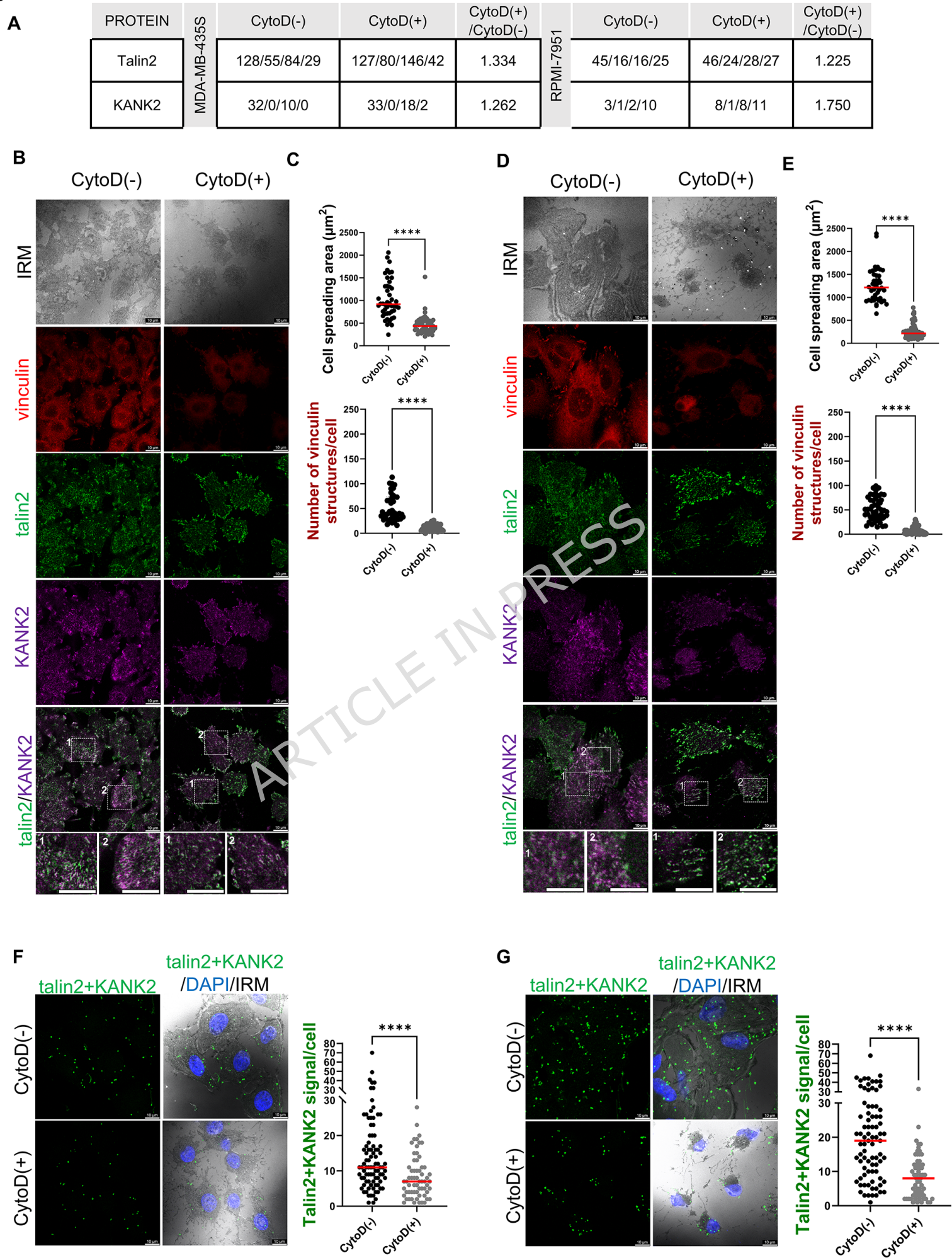


Fig. 4

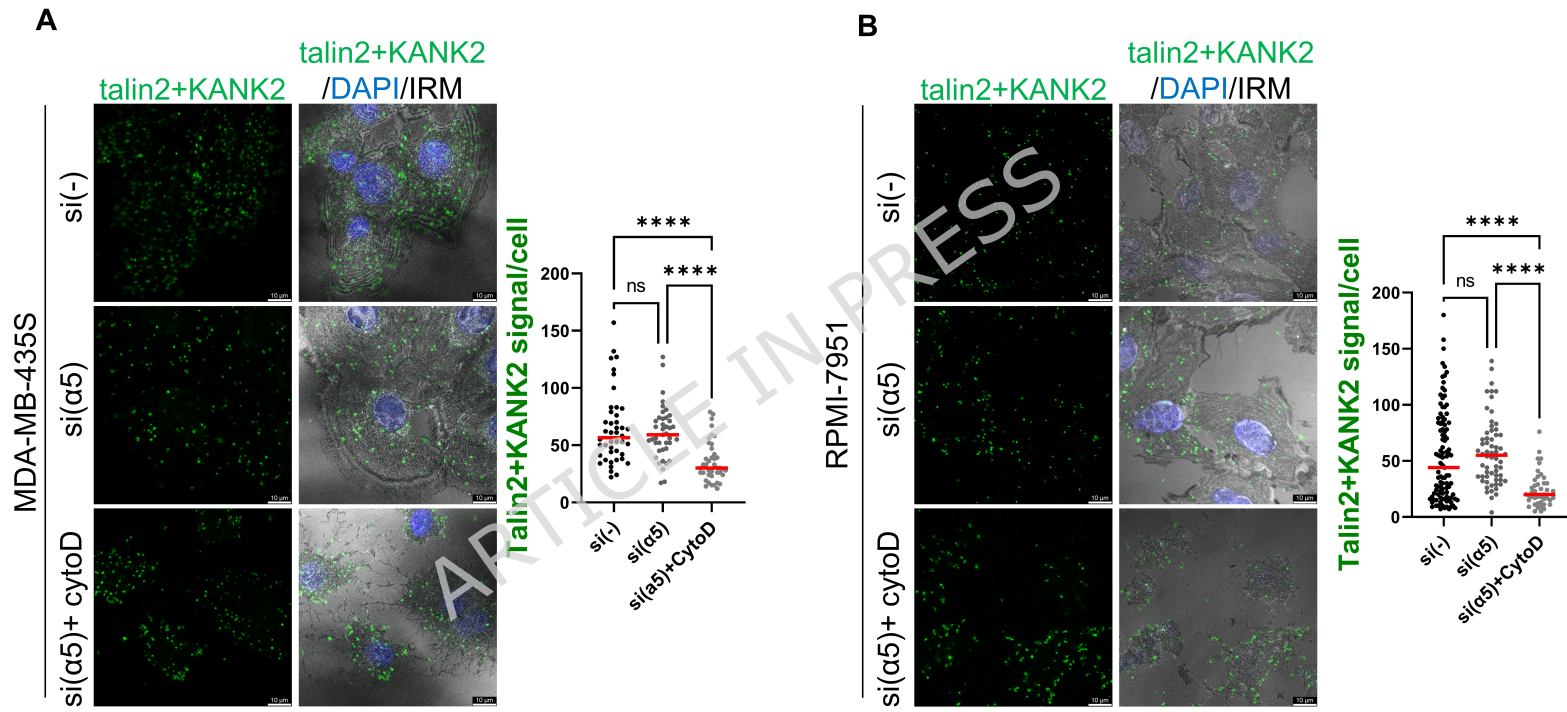


Fig. 5

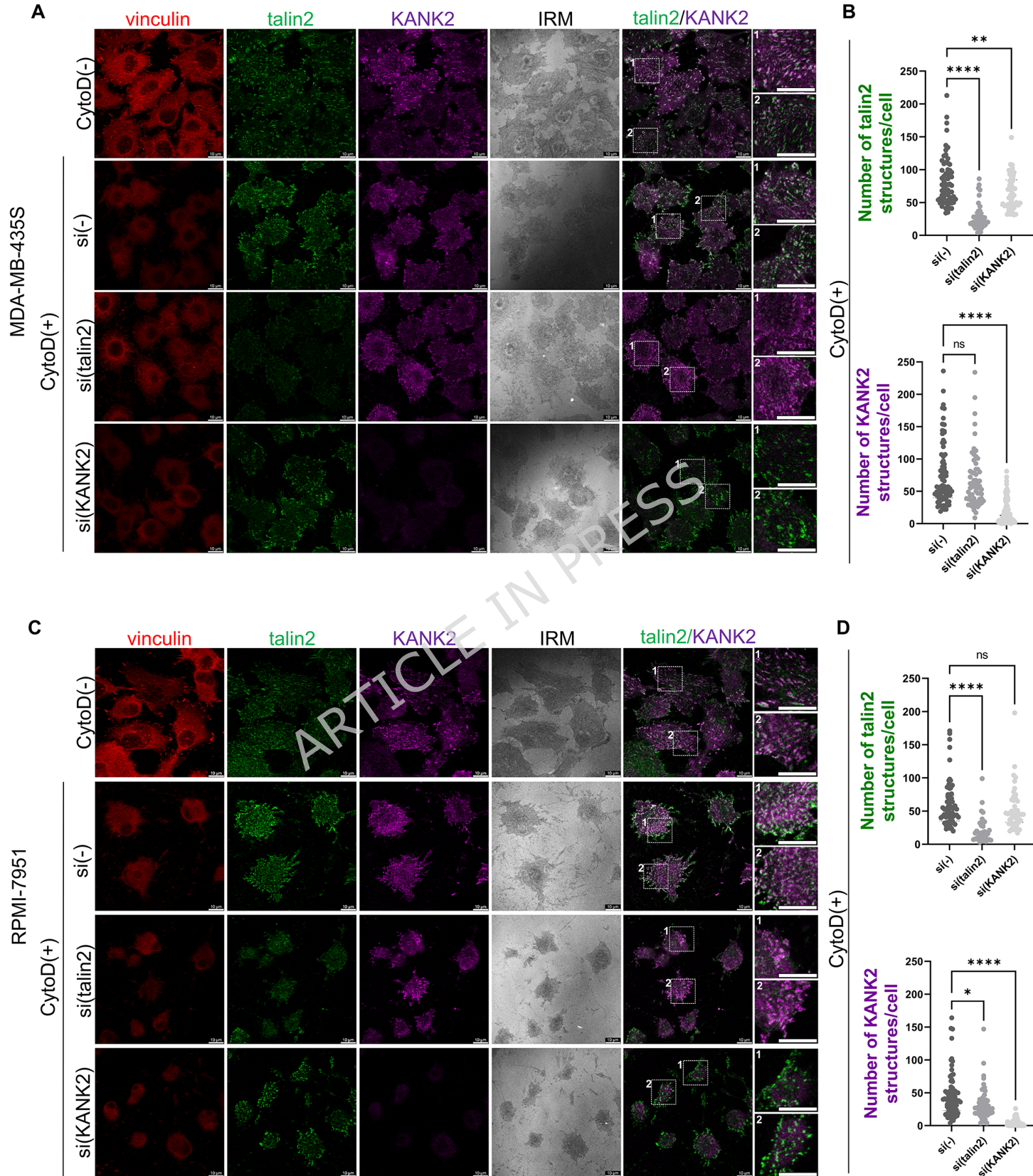
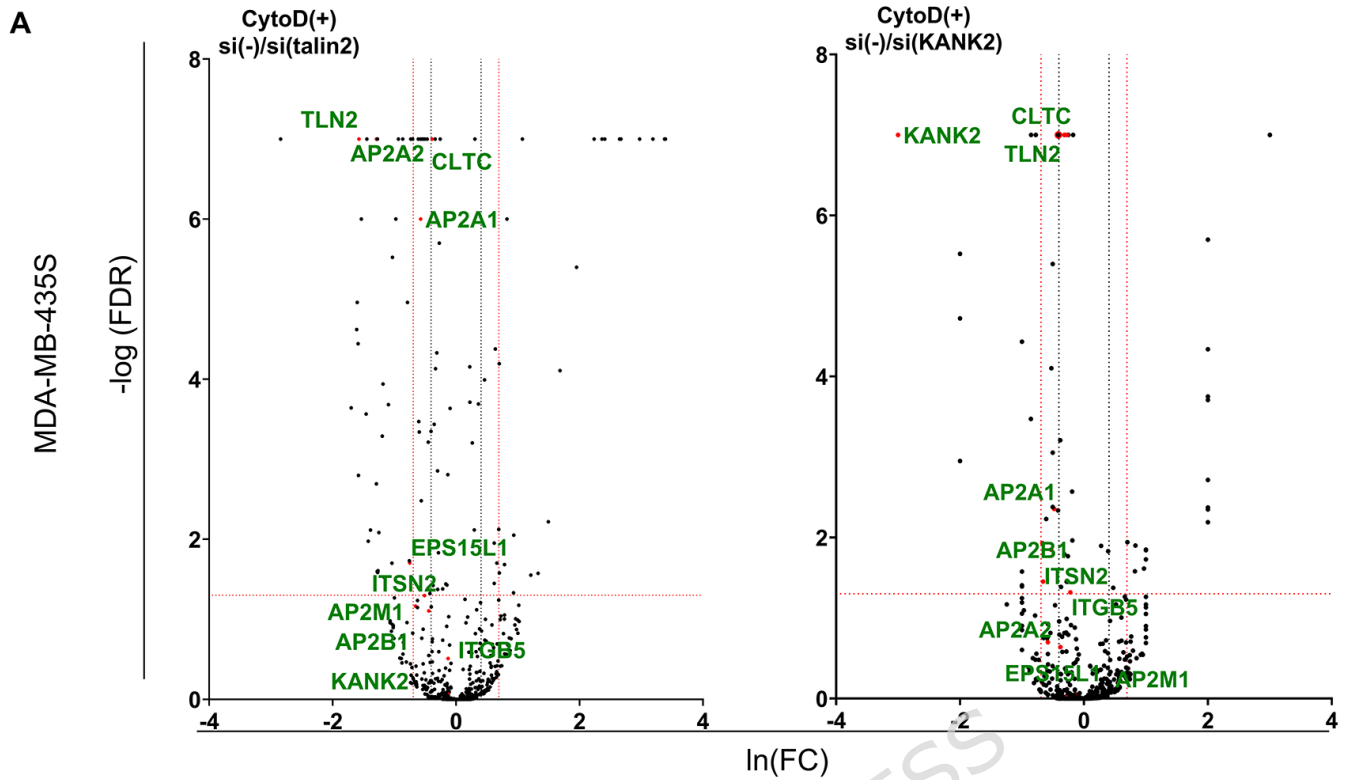
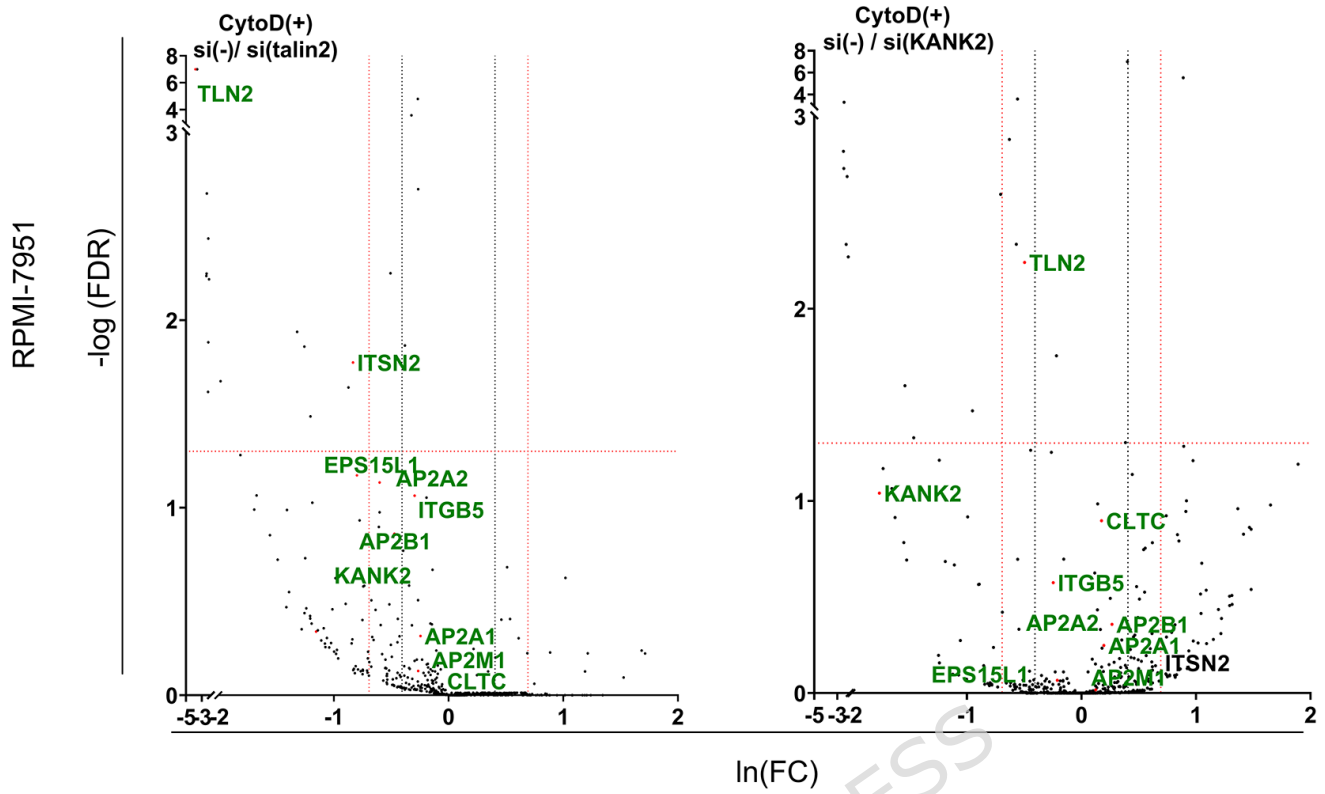


Fig. 6

**B**

PROTEIN		si(-)	si(talin2)	si(talin2) /si(-)	si(KANK2)	si(KANK2) /si(-)
AP2A1	MDA-MB-435S	18/23/19	9/15/13	0.615	6/19/14	0.650
AP2A2		12/16/0	0/7/0	0.247	0/12/8	0.710
AP2B1		7/10/10	7/5/7	0.700	1/10/4	0.555
AP2M1		4 /6/4	2/3/3	0.565	2/6/7	1.087
CLTC		101/111/99	72/80/75	0.730	47/95/72	0.688
EPS15L1		11/6/2	4/4/2	0.524	7/6/3	0.841
Integrin $\beta$ 5		57/57/54	45/56/57	0.939	37/49/54	0.832
ITSN2		16/6/4	8/8/1	0.651	3/9/2	0.535
KANK2		16/12/5	19/5/6	0.909	0/0/0	NA*
Talin2		181/156/144	35/41/32	0.225	131/127/123	0.793

C



D

PROTEIN		si(-)	si(talin2)	si(talin2) /si(-)	si(KANK2)	si(KANK2) /si(-)
AP2A1	RPMI-7951	17/50	11 /37	0.727	26/52	1.182
AP2A2		9/32	0 /19	0.450	13/30	1.050
AP2B1		11/34	4 /22	0.591	14/42	1.273
AP2M1		5/17	4 /12	0.727	5/18	1
CLTC		78/132	72 /111	0.867	72/157	1.124
EPS15L1		8/16	4 /6	0.417	6/15	0.833
Integrin $\beta$ 5		47/60	34 /39	0.679	42/38	0.755
ITSN2		5/29	2 /12	0.412	2/30	0.941
KANK2		3/7	3 /1	0.400	0/0	NA*
Talin2		30/46	0/0	NA*	12/32	0.579